Acoustic Monitoring of Floating Offshore Wind Turbines

Elizabeth Hauschild, Ocean Engineering and Rose Walker, Ocean Engineering
Department of Ocean Engineering, University of New Hampshire
Advisors: Martin Wosnik, Tom Weber
Industry Partner: Jerica Nolte (Attentive Energy)

May 13, 2022

Table of Contents

Abstract ***3***
Introduction ***3***
Background ***3***
Goal ***8***
Approach ***8***
Methods ***8***
Mooring Chain **8**
Turbine Generator **11**
Results and Discussion ***12***
Mooring Chain Experiments **12**
Turbine Generator Experiments **18**
Conclusions ***22***
Mooring Chain Experiments **22**
Turbine Generator Experiments **22**
Recommendations for Future Work ***23***
Acknowledgements ***23***
Appendix ***23***
References ***26***

Acronyms

Abbreviation	**Explanation**
AE	Acoustic Emissions
FWT	Floating Wind Turbines
O&M	Operations and Maintenance
SHM	Structural Health Monitoring
STS	Station Keeping System
TLP	Tension-Leg Platform
WTG	Wind Turbine Generator

Abstract

Offshore wind turbines are a rising technology in the renewable energy market worldwide as a method for electricity generation. The primary design for offshore wind turbines is fixed-bottom structures, which can be built in water depths up to 60 m. However, the National Renewable Energy Laboratory (NREL) estimates that 80% of global offshore wind resources exist in waters with depths greater than 60 m, therefore many companies are turning towards floating structures as a solution (Ezzaidi et al., 2017). One great challenge to this industry will be determining when to conduct maintenance and inspection on these structures. To address this challenge, this project investigated the feasibility of using acoustic emissions for the structural health monitoring of mooring chains and turbine generators of floating offshore wind platforms. This was done by comparing the acoustic emissions of heathy and damaged physical models for a mooring chain and turbine generator. Findings from this project determined that acoustic emissions testing for a mooring chain may not be recommended as a stand-alone method of structural health monitoring, but it may be more reliable for turbine generator monitoring. There are many limitations to using acoustic monitoring for the mooring chain and turbine generator of floating offshore wind turbines, however findings from this project will help to direct the next steps of acoustic emissions monitoring.

Introduction

As offshore wind becomes increasingly popular around the globe, there has been an effort to design floating structures to access the stronger wind resources in deeper waters. One of the many challenges of floating offshore wind farms is the optimization in scheduling operations and maintenance (O&M). Routinely scheduled structural health monitoring (SHM) can be done on-site visually, however it is expensive, dangerous, and time consuming. This research project aims to investigate the use of remote acoustic systems for condition-based monitoring for floating wind turbines (FWTs). With the help of industry partner, Attentive Energy, tests were performed to investigate the feasibility of using acoustics for routine SHM of mooring chains and for turbine generators of FWTs.

Background

Horizontal-axis wind turbines generate electricity using wind energy. The typical machine configuration consists of 2-3 blades facing into the wind extending from a central hub. As wind applies lift and drag along the blades, the rotational force, or torque, spins a shaft connected to a generator which produces electricity. The speed of the blades is modulated by adjusting the angle of attack, i.e., the pitch of the blade to the wind. As wind increases, the power produced initially increases along a cubic curve. An example power curve developed to model the performance of a GAMESA G52-850 wind turbine is shown in Figure 1, where the power output increases cubically with windspeed until around 12 m/s (Ezzaidi et al., 2017). When the generator reaches its rated power, blade pitch control is used to limit to limit the power output as the wind speed continues to increase (NREL Learning, 2020). As shown in Figure 1, when the wind speeds exceed 12 m/s, the rated power of the turbine is maintained at 850 kW.

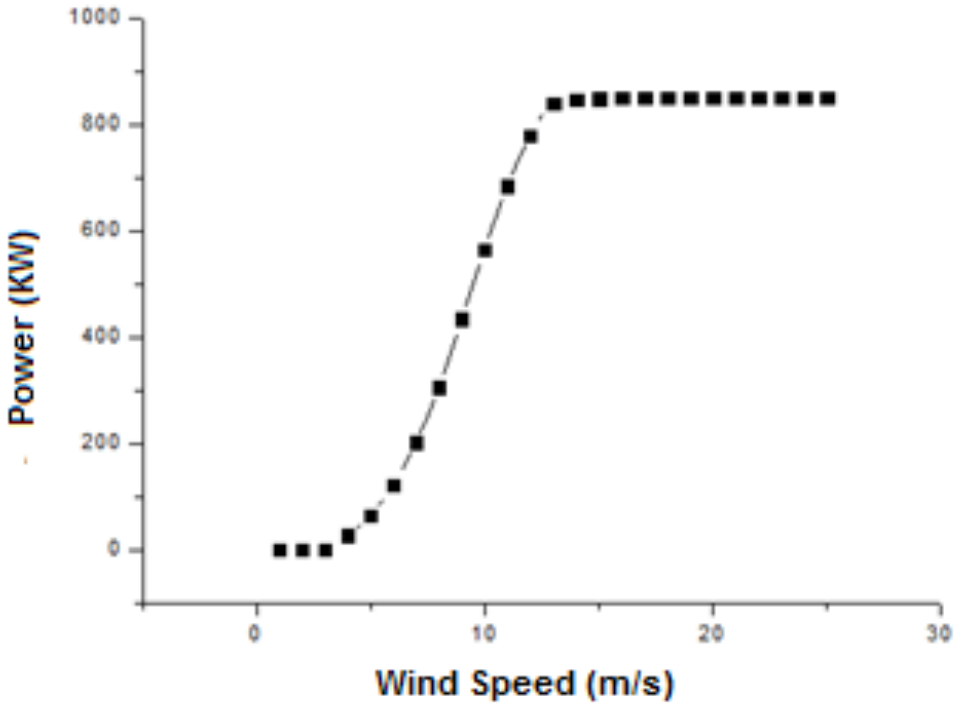

Figure 1: Power curve of G52-850 wind turbine (Ezzaidi et al., 2017).

The power output of a wind turbine can be limited by wind speed, hub height, the blade diameter, or sweep area, electrical efficiency, and space requirements for equipment in the wind turbine generator (WTG). To increase the WTGs power rating, WTGs are built with larger generators, hub heights, and sweep area. As turbines increase in size, however, they must be spaced farther apart in their array to allow for the wind to re-establish itself between each machine to resolve the turbulence caused by the wake effects (NREL Learning, 2020).

Onshore wind turbines struggle to meet the energy demands of the United States. The United States Energy Information Administration recorded the energy consumption in the US was 3.9 trillion kilowatt-hours (kWh) in 2021, and consumption is predicted to increase through the future (*Electricity Explained - U.S. Energy Information Administration (EIA)*, 2022). The largest onshore wind turbine built is rated for 4.8 MW power output which produces around 6 million kWh per year. To match this demand, onshore turbines would require a large amount of space, impeding on preserved land, historical spaces and even invading into citizens' backyards. To solve this problem, the future of wind energy is moving offshore where space resources are abundant and turbines will be out of sight, yet still have the ability and access to power the highest load centers of the United States located near the coasts.

The benefits of implementing offshore wind farms outweigh more than just resolving the lack of land resources. Offshore wind blows stronger and more consistently than onshore wind and with 80% of Americans living near a coast, the resources match up with the energy demands (Abbelurg et al., 2014). Without the size limitations of onshore machines due to transportation constraints, offshore turbines have the potential to be twice the size or greater than land turbines.

Just one 15 MW turbine could power 4,000 to 4,500 US homes. Globally, over 27,000 MW of wind power is installed on fixed-bottom turbines, but turbines can only be fixed to the seafloor in water depths up to 60 meters, and 80% of offshore wind resources are in waters greater than 60 meters (Ezzaidi et al., 2017, Abbelurg et al., 2014). As there are only so many locations suitable for offshore fixed wind, it is necessary to engineer efficient floating wind turbines to continue to capitalize on the strength and abundance of offshore wind energy.

The three basic designs for offshore floating platforms are spars, semi-submersibles, and tension-leg platforms (TLP), shown in Figure 2 (Brookes et al., 2014). A spar maintains stability through a heavy ballast below the center of buoyancy. The spar design is not compatible with every port due to its depth requirements and large draft. A semisubmersible uses a wide distribution of buoyancy at the water plane to establish stability. With a wide base, these platforms encounter more wave energy and weather exposure. The tension-leg platform design relies on the tension of several mooring lines attached to a submerged buoyancy tank to achieve high static stability during operation (NREL Learning, 2020).

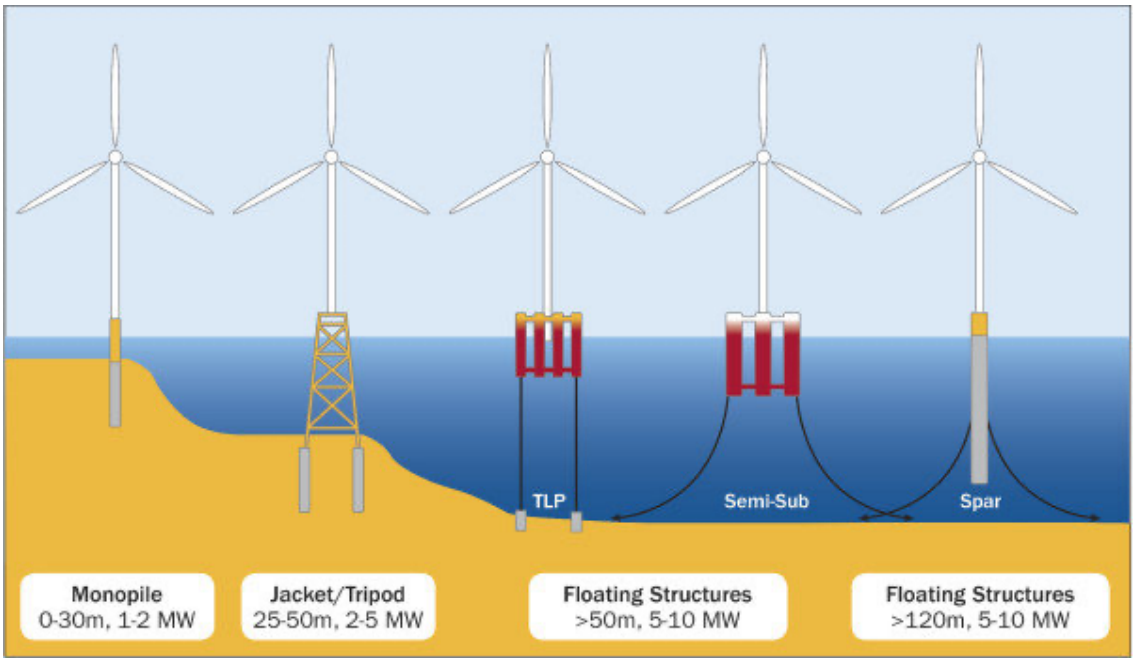

Figure 2: Floating turbine designs (Brookes et al., 2014).

Currently, several offshore floating wind projects are being constructed and installed in various regions of the world's oceans. Hywind Scotland is the world's first floating pre-commercial wind farm, constructed in 2017. A photo of the farm is shown in Figure 3. The project deployed five, 6 MW spar turbines in a "park" configuration with the ability to power 20,000 homes in the United Kingdom, or 400,000 kWh of energy. Following Hywind Scotland, Windfloat Atlantic began installation in Portugal in 2019. Five additional projects began design in 2020 in Spain, Sweden, and the UK and four more followed in 2021 based in France. The largest floating pre-commercial wind project installed today is Kincardine, a 49 MW capacity farm based in the UK, and Hywind Tampen, an 88 MW farm is currently being built in Norway and is to be installed in 2022 (*Floating Offshore Wind Energy: A Policy Blueprint for Europe*, 2016).

Figure 3: Hywind Scotland (*Floating Offshore Wind Energy: A Policy Blueprint for Europe, 2016).*

An area of optimization of floating offshore wind platforms is scheduling maintenance. A small repair can be made in the field using service vessels, but larger repairs require offshore cranes and, in some cases, disconnecting the entire structure and towing it to shore. Regardless of the scale of the repair, both large and small operations are costly, including the cost of energy lost in shutting off the turbine to access it. Since it may not always be clear why or when a turbine needs repair, regular and routine investigation of the machinery is required, taking more time and cost.

Repairs that pose a particular challenge to investigate include faults inside the turbine and underwater systems. The location of several key components of a turbine is shown in Figure 4. Within the nacelle, or the center station of the blade assembly, are the generators, motors and in some machines, the gear box. Below the surface of the water, there is an array of electrical cables and station keeping systems. The station keeping system (SKS) includes the mooring and anchor system of synthetic mooring lines, chains, wires, and anchors that experience wear and are possible points of failure (NREL Learning, 2020).

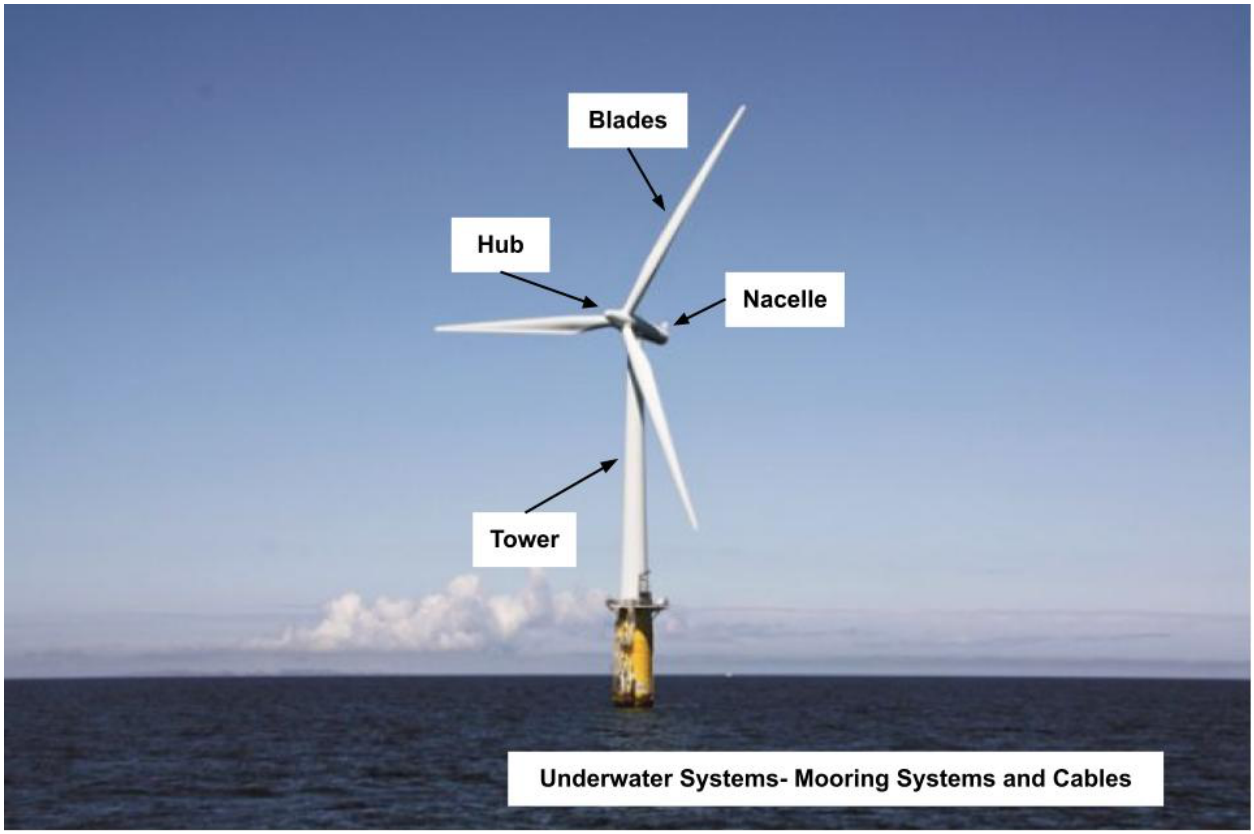

Figure 4: Labeled major components of offshore wind turbine.

Current methods of remote SHM include the use of strain gauges, inertial measurement unit sensors, and visual inspection performed by autonomous underwater vehicles. Wind turbines currently utilize accelerometers to measure changes in velocity and vibration of turbine components, including bearings and the main generator output shafts. This vibration data is used to monitor changes over time to predict failures (Manz, 2020). Strain gauges are used for monitoring the structural health of turbine blades and are being integrated into mooring systems. However, with both accelerometers and strain gauges, there are limitations to what can be monitored and how early failures can be predicted. In addition, these methods are limited to their local stress or inspection fields and may not be the most effective methods of SHM (Martinez-Luengo et al., 2016). Therefore, this research investigated the use of acoustic emissions technology as a method of condition-based monitoring.

Acoustic emission (AE) monitoring is a passive structural health monitoring (SHM) technique that uses the analysis of sound intensity and frequency to identify failure in a structure (Tonelli et al., 2020, Mba, 2006). In the same ways a user can detect when there is something wrong with a vacuum cleaner or a car based on a change in the way it sounds, it may be possible that the health of several components of a FWT can be determined by its acoustic emissions. This could allow for the monitoring of components such as the mooring line or turbine generator. The use of AE technologies for SHM of FWTs has the potential to reduce the cost of investigating repairs and the need for frequent visual inspections by providing remote data on the turbine's health.

Goal

The goal of this project is to investigate the feasibility of using acoustics for condition-based monitoring of offshore floating wind platforms. Likely and detectable modes of failure include failure, wear, or cracks in mooring lines or turbine generators. The goal is to develop a passive analysis using remote microphone listening and data acquisition to evaluate the health of the FTW's mooring chain and turbine generator.

Approach

A series of tests were performed on simplified physical model representations of the complex systems of a mooring chain and turbine generator. The acoustic emissions of each test in air were recorded using a Blue Yeti Stereo Microphone, sampling at 22,050 Hz and 48,000 Hz. The time series were transformed to the frequency domain, processed, and analyzed using MATLAB.

For the mooring chain, multiple lengths of ½ trade size steel chain with 13.50 mm thickness was used to represent a FWT mooring chain. One end was fixed in a vice grip, and the other end was loaded with weight to induce tension, and the chain was acoustically excited by swinging. The chain emissions for the following conditions were recorded: varying chain length (two links, five links, ten links), varying chain load (2.27 kg, 4.53 kg, 15.88 kg), and introducing a notch cut (defect) into the chain.

The mooring chain tests considered varied chain load to determine how different loading on the mooring chain could affect the interaction between two isolated chain links. It was hypothesized that the amplitude of the chain frequency response would be most impacted due to the increased force at the connection point between the links. A mooring chain test with varied chain lengths was also performed to assess how increasing the number of chain links changes the frequency spectra. Findings from these two tests are used to determine how applicable the results of the 2-link and 5-link healthy and damaged tests are to other mooring configurations.

A fan was used to represent a turbine generator. The fan is 120 x 120 x 38 mm and operates at 2600 RPM. The fan emissions for the following conditions were recorded: healthy fan, uneven loading on one fan blade, and tampered ball bearings using salt. The frequency spectrums were compiled and compared to one another to determine if the varying conditions could be observed in their frequency spectrums.

Methods

Mooring Chain

All acoustic tests were performed in a lab setting with electrical and industrial ambient noise. Small steel chain, used to represent a mooring chain was cut into sections using an electrical saw. Two, 2-link sections were cut, two 5-link sections were cut, and one 10-link section of chain was cut from the original longer length of chain.

Figure 5: 2-link chain experimental setup.

The lab setup contained a vice grip fixed to the end of one of the lab benches. For each trial, one end of the chain being examined was fastened in the vice grip and the other was tied to a small diameter synthetic line. Cast-iron weight was added to the line to induce tension on the links of the chain. The chain was acoustically excited to emit noise by displacing the weight 60 degrees and releasing it, allowing the chain to swing like a pendulum. As the chain swung, it emitted a nonpredictable array of sounds that were characterized as either a “squeak” or a “clunk”. A photo of the 2-link chain experimental setup in the vice grip with a weight is shown in Figure 5.

The test matrix shown in Table 1 was developed for the several conditions to be explored using the chain. The first condition explored was the impact of varying chain length on the acoustic emissions of the chain. The acoustic emissions were tested on the 2-link chain, 5-link chain, and the 10-link chain using a 2.27 kg weight. Varying chain load was tested on the 2-link chain using a 2.27 kg, 4.53 kg, and 15.88 kg weight. Finally, introducing a notch cut (defect) into the chain was explored on both the 2- and 5-link chains. A 6.8 mm notch was cut using the electric saw in the center of the chain. A photo of the notched and healthy chains is shown in Figure 6.

Table 1: Test Matrix for Chain Experiments.

	Variables					
	Chain Length	Chain Load (kg)			Chain Health	
Test Series						
Varying Length	2-link	2.27			No defect	
	5-link					
	10-link					
Varying Load	2-link	2.27	4.53	15.88	No defect	
	5-link					
Adding a Defect	2-link	2.27			No defect	With defect
	5-link					

Figure 6: Healthy and notched 2- and 5-link chains.

The sounds emitted from by the chain were recorded using the Yeti Microphone, which was placed on the lab bench 6 inches away from the vice grip. The microphone was operated using MATLAB and a protocol and code were written for the purpose of the experiments (see Appendix). This program automatically clipped 0.2 seconds from the beginning of each recording to eliminate the microphone startup transient. For each trial, the microphone was used to record a 15-second-long observation of the ambient noise present in the lab before moving the

chain. The ambient noise was saved for each section of the test matrix and then the frequency spectra were averaged. Following the ambient noise recording, the MATLAB code was used to record 15-second-long trials of the chain noise for each test. To do this, the weight was released from displacement at the same time as the audio recording began. The chain swung while the microphone recorded its noise for 15 seconds. When the audio recording was complete, the chain was stopped, and the weight was brought back to the position of initial displacement so that another recording could be performed. For each section of the test matrix, one ambient noise trial was recorded, and 15 chain noise trials were recorded.

Using MATLAB, the audio data time series data was transformed to the frequency domain using the periodogram function. The frequency spectra of all 15 trials of each test were averaged together and then smoothed using Savitzky-Golay filtering. The processed spectrograms for each trial were plotted against the ambient noise and each another so that differences in their amplitudes and frequencies could be compared.

Turbine Generator

The turbine generator experiments were performed and processed similarly to the mooring chain experiments. A fan used to model the rotating components of a generator was subjected to three trials: healthy, unevenly loaded, and tampered ball bearings. The same MATLAB code and microphone recorded the ambient and fan noise data, but number of trials was reduced from 15 to five because the fan emitted more predictable and repeatable sounds.

Figure 7: Fan and microphone experimental setup.

Table 2 shows the test matrix for the turbine generator experiments. The healthy fan was recorded by placing the fan on the lab bench in front of the microphone shown in Figure 7. The fan was turned on and recorded five times, for 15 seconds each time. Then, uneven loading was explored by adding weighed masses of tape to the tip of one of the fan blades. The load cases tested were 0.05 g, 0.10 g and 0.50 g. Finally, the ball bearings of the fan were tampered with by

deconstructing the fan, removing the bearing shield, adding salt to the inside of the bearings, and reconstructing the fan. A photo of the fan deconstruction and bearing tampering is shown in Figure 8.

Table 2: Test Matrix for Turbine Generator Experiments.

Test Series	Load (g)	Salt in Bearings
Control	None	No
Uneven Loading	0.05	No
	0.1	No
	0.5	No
Tampered Ball Bearings	None	Yes

Figure 8: Group member Rose Walker tampering with the fan.

The data was processed the same way as outlined for the mooring chain experiment and the spectrograms for each test were plotted against one another to compare their frequency emission spectrums.

Results and Discussion

Mooring Chain Experiments

In all trials for the mooring chains, there was an audible difference between different runs, even if all variables were held constant. Some of the sounds can be described as a squeak, while other sounds can be described as a grinding or a "clunking" noise. On other trials, the chain would make little to no noise. Figures 9 through 12 display the frequency spectra of the mooring chain experiments. In all these figures, the frequency range displayed is clipped for clarity of the low-

frequency AE response. Any data outside of the displayed range is not significant. In all these plots, ambient noise is plotted for comparison to AE of the chain movement.

Figure 9 displays the frequency spectrum of the AE comparison of the 2-link chain with a 2.27 kg weight, 4.53 weight, and 15.88 kg weight. In the low frequency between 30 and 80 Hz, all loading cases result in high peaks with a maximum occurring at 65 Hz. The 2.27 kg weight load and 4.53 kg weight load experience peaks at 100 Hz and 120 Hz, but the larger loading condition does not, Furthermore, between 340 Hz and 420 Hz, the spectra for the 2.27 kg load and the 4.53 kg weight appears similar with differences primarily in the magnitude of peaks. Lastly, between 510 Hz and 540 Hz, all three loading cases experience peaks. A visual tabulation of the frequency ranges and spikes that occurred for each loading case is shown in Table 3. The frequencies amplitudes present for each case are filled in the table.

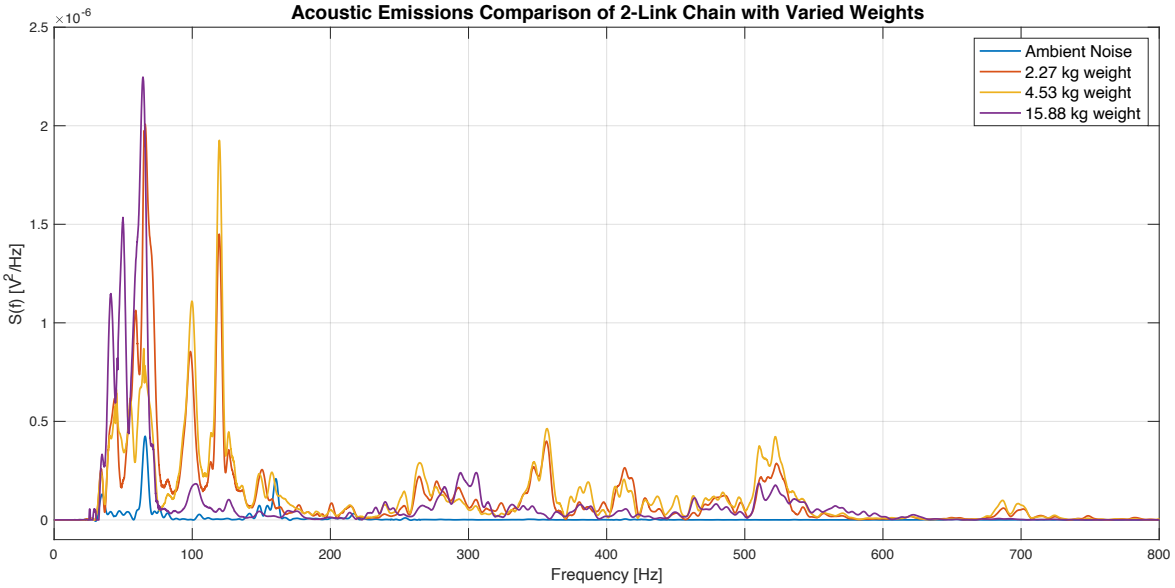

Figure 9: Frequency plot of AE of 2-link chain with 2.27 kg, 4.53 kg, and 15.88 kg load.

Table 3: Observable Frequency Response for Each Load Case.

2-Link Chain with Varied Weights					
	Most Apparent Frequencies with Amplitudes				
Load Case (kg)	65 Hz	100 Hz	120 Hz	340 Hz-420Hz	510Hz-540Hz
2.27	2.01×10^{-6} V^2/Hz	8.52×10^{-7} V^2/Hz	1.45×10^{-6} V^2/Hz	4.62×10^{-7} V^2/Hz	2.86×10^{-7} V^2/Hz
4.53	8.69×10^{-7} V^2/Hz	1.11×10^{-6} V^2/Hz	1.93×10^{-6} V^2/Hz	3.99×10^{-7} V^2/Hz	4.22×10^{-7} V^2/Hz
15.88	2.25×10^{-6} V^2/Hz	1.78×10^{-7} V^2/Hz			1.75×10^{-7} V^2/Hz

Figure 10 shows the AE frequency spectrum of 3 lengths of chain, all with 2.27 kg weight. The chain lengths tested were 2-links, 5-links, and 10-links. Most of the AE response occurs in the 30

Hz to 165 Hz range. In all chain length cases, there is a spike in the frequency spectrum at 60 Hz, 97 Hz, and 116 Hz. The magnitude of these spikes is higher for the 5-link chain and the 10-link chain compared to the 2-link chain, listed in Table 4.

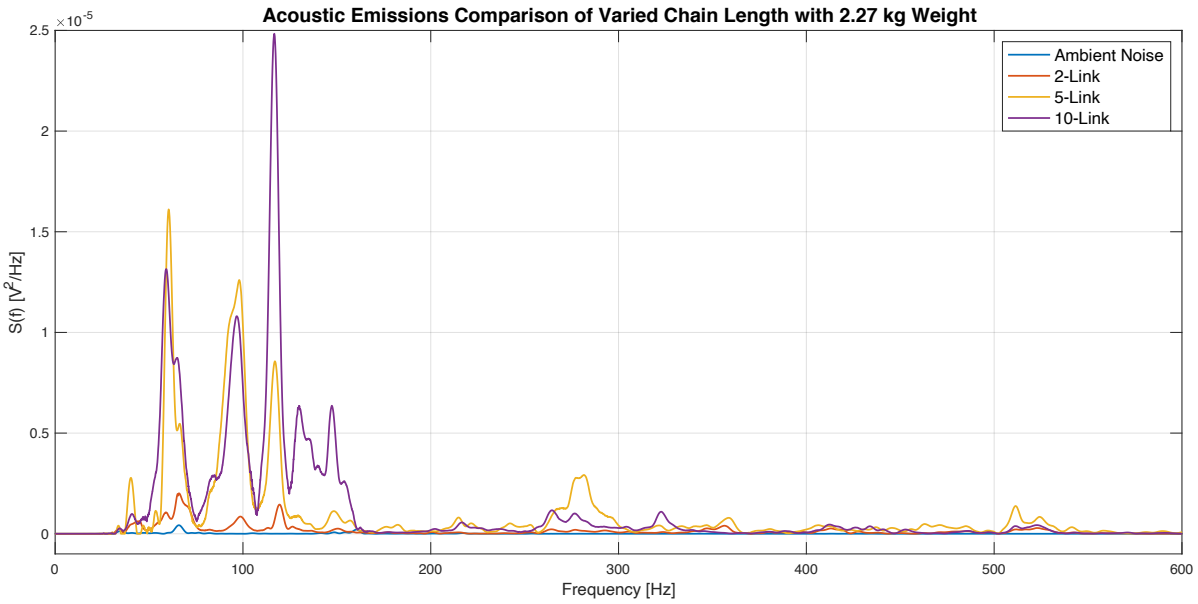

Figure 10: Frequency plot of AE of 2-link, 5-link, and 10-link chain with 2.29 kg weight.

Table 4: Observable Frequency Response for Each Chain Length.

Varying Chain Length			
	Most Apparent Frequencies with Amplitudes		
Length	60 Hz	97 Hz	116 Hz
2-Link	$1.95\text{x}10^{-6}$ V^2/Hz	$8.22\text{x}10^{-7}$ V^2/Hz	$1.45\text{x}10^{-6}$ V^2/Hz
5-Link	$1.61\text{x}10^{-5}$ V^2/Hz	$1.25\text{x}10^{-5}$ V^2/Hz	$8.51\text{x}10^{-6}$ V^2/Hz
10-Link	$1.35\text{x}10^{-5}$ V^2/Hz	$1.07\text{x}10^{-5}$ V^2/Hz	$2.45\text{x}10^{-5}$ V^2/Hz

The following figures, Figure 11 and Figure 12, display the frequency spectrum of unbroken chains compared to broken chains of the same length and loading. Figure 11 displays the AE comparison of broken and unbroken 2-link chains with a 2.27 kg load. As in Figure 9 and Figure 10, there is a significant AE response in the range of 30 Hz to 165 Hz, with peaks at 60 Hz, 97 Hz, and 120 Hz for both the unbroken and broken chain test cases. There is a significant difference in acoustic response from 215 Hz to 290 Hz for the unbroken and broken chain. Here, the power spectral density of the broken chain reaches magnitudes of $1.4\text{x}10^{-6}$ V^2/Hz at 264 Hz, where the maximum unbroken chain power spectral density only reaches $2.2\text{x}10^{-7}$ V^2/Hz at the same frequency. At 240 Hz, the broken chain has a peak equal to $1.3\text{x}10^{-6}$ V^2/Hz, and the unbroken chain is two orders of magnitude smaller. From 394 Hz to 423 Hz and 473 Hz to 540 Hz, the power spectral density is similar for the unbroken and broken cases with slight differences in magnitude. The broken chain also has peaks at 448 Hz and 463 Hz, where the unbroken chain does not. These frequencies and amplitudes are organized in Table 4.

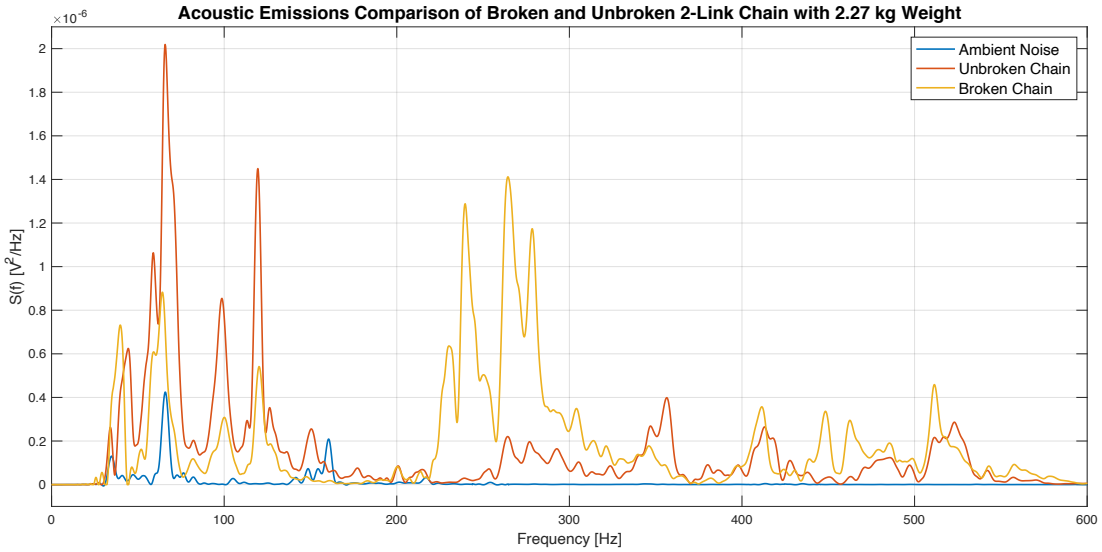

Figure 11: Frequency plot comparison of 2-link unbroken and broken chain.

Table 4: Observable Frequency Response for Broken and Unbroken 2-Link Chain.

Broken and Unbroken 2-Link Chain					
	Most Apparent Frequencies (Hz) with Amplitudes				
	30 Hz	60 Hz	97 Hz	120 Hz	215Hz-290Hz
Unbroken	0.6×10^{-6} V^2/Hz	2.0×10^{-6} V^2/Hz	0.85×10^{-6} V^2/Hz	1.45×10^{-6} V^2/Hz	1.4×10^{-6} V^2/Hz
Broken	0.7×10^{-6} V^2/Hz	0.8×10^{-6} V^2/Hz	0.3×10^{-6} V2/Hz	0.55×10^{-6} V^2/Hz	0.01×10^{-6} V^2/Hz

Figure 12 displays the AE comparison of the broken and unbroken 5-link chain with a 2.27 kg load. For the unbroken chain, peaks occur at 60 Hz, 97 Hz, and 116 Hz. The broken chain has peaks with smaller magnitude at 97 Hz and at 122 Hz. The magnitude of the broken chain power spectral density does not exceed 3.5×10^{-7} V^2/Hz for any frequency greater than 180 Hz. The unbroken chain produces an increase in power spectral density from 260 Hz to 300 Hz. These frequencies and amplitudes are listed in Table 5.

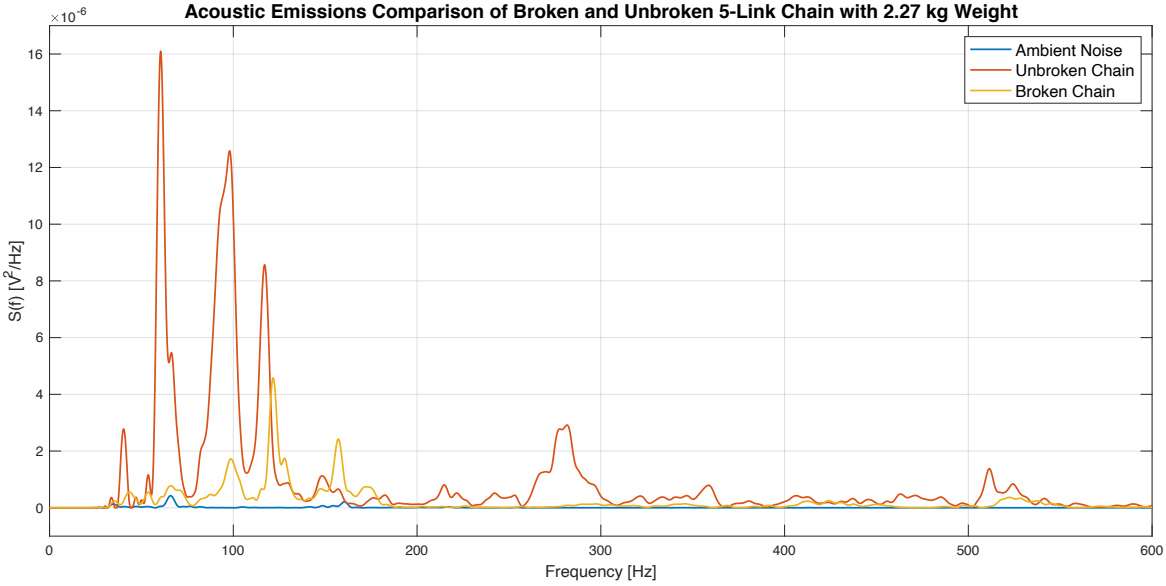

Figure 12: Frequency plot comparison of 5-link unbroken and broken chain.

Table 5: Observable Frequency Response for Broken and Unbroken 5-Link Chain.

Broken and Unbroken 5-Link Chain				
	Most Apparent Frequencies (Hz) with Amplitudes			
	60 Hz	97 Hz	122 Hz	260 Hz
Unbroken	16×10^{-6} V^2/Hz	12.7×10^{-6} V^2/Hz	8.7×10^{-6} V^2/Hz	3.0×10^{-6} V^2/Hz
Broken	0.7×10^{-6} V^2/Hz	1.9×10^{-6} V^2/Hz	4.7×10^{-6} V^2/Hz	0.03×10^{-6} V^2/Hz

The results of Figure 9 and Figure 10 are important in determining the applicability of using AE monitoring for the structural health monitoring of mooring chains. In theory, if structurally healthy mooring chains have similar frequency patterns, it is much easier to apply the findings of these initial feasibility tests to other loading and length cases. Otherwise, determining the frequency of a specific mooring configuration in an unbroken state may be necessary, or AE monitoring is not feasible at all. Figure 9 shows that all three loading cases produce similar results in the low frequency, between 30 Hz and 80 Hz, and in the 510 Hz to 540 Hz range, with some differences in magnitude. Furthermore, some loading cases, namely the 2.27 kg load and the 4.53 kg load, exhibit the same patterns in the frequency range of 340 Hz to 420 Hz, but these results do not match that of the largest loading case. From this, it can be concluded that, holding all other variables constant, the attached load of a chain will affect the AE spectrum after a certain load is exceeded.

Figure 10 also serves to determine the way that changing the variables in an unbroken chain affect the acoustic emissions. Again, in the lower frequency range of 30 Hz to 120 Hz, the different test cases exhibit peaks at the same frequencies. There is, however, a significant difference in magnitude for these results. It is undetermined if this is a result of an error in data collection or a natural response to change in chain length. In higher frequencies, the power

spectral density is relatively low. There is a long spike in power spectral density at 500 Hz to 540 Hz, which also appeared in Figure 9.

From these initial tests, it is determined that there are some limitations to applying findings to all mooring configurations and cases. However, there are consistencies through these tests that, if significantly changed, would indicate some failure in a mooring chain. Figure 11 and Figure 12 display the results of the more specific cases of using AE for chain monitoring, where all variables were held constant except for an induced defect in one of the links.

Figure 11 displays the frequency spectrum for an unbroken and broken 2-link chain. As with the initial tests, the frequency response in the 30 Hz to 120 Hz is consistent in the broken chain case. The most significant differences in the power spectral density are occurring in the 215 Hz to 290 Hz range. The difference in these plots is significant and detectable, and if the acoustic emissions of the mooring system were known, a difference of this magnitude could be a signal that something is wrong. However, in Figures 9 and 10, it was difficult to determine any sort of pattern in frequency spikes in this range. So, unless the magnitude difference is considerable, the results of this figure may be difficult to draw any general conclusion about the behavior of the broken chain.

Furthering the complexity, Figure 12, the comparison of the unbroken and broken 5-link chain, the 5-link broken chain behaves very differently from the 2-link chain. In order to more clearly illustrate this phenomenon, Figure 13, below, displays the frequency spectrum of only the broken 2-link chain and the broken 5-link chain.

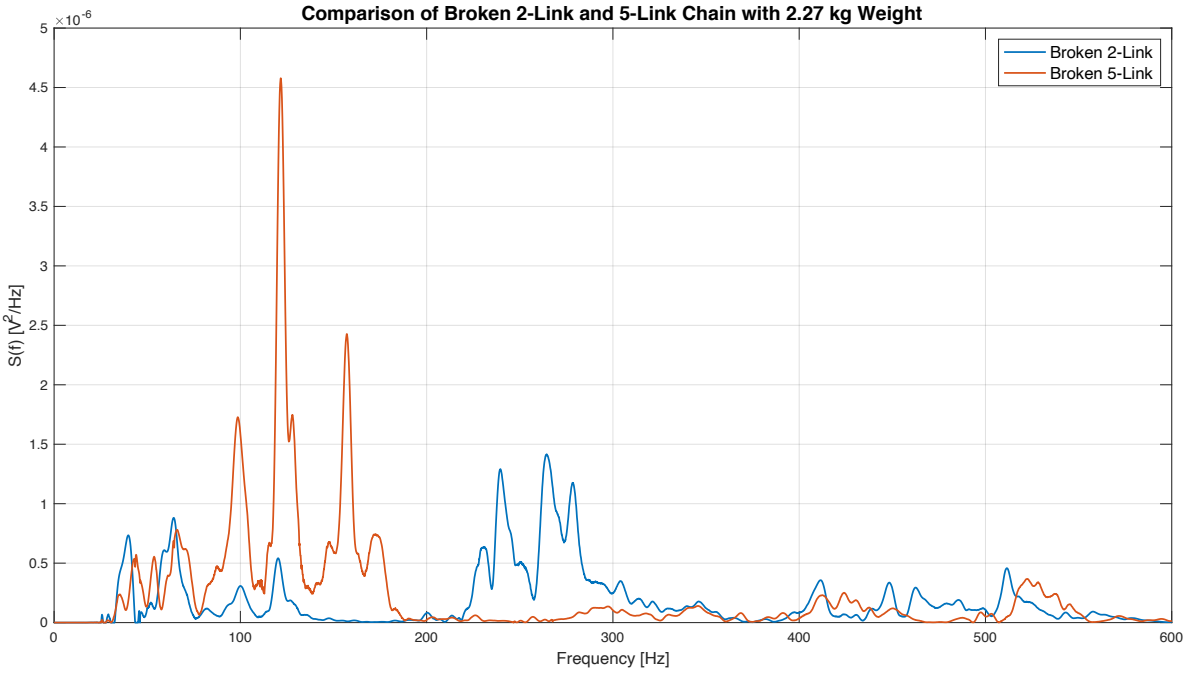

Figure 13: Frequency plot of the AE difference of the broken 2-link and broken 5-link chain.

In Figure 13, the most difference occurs between 140 Hz and 320 Hz. Because the acoustic response is different between these two broken cases, it is difficult to determine a pattern for breaking. Differences may be caused by the induced break not being the same for the 2-link chain and the 5-link chain, as it was done manually. However, as previously mentioned, a distinguishable difference between known AE of an unbroken chain and the same chain with an induced break may still be informative about the condition of the chain, as seen in Figure 11.

In Figure 12, the frequency plot comparison of the 5-link unbroken and broken chain is given. The power spectral density of the broken chain varies greatly in magnitude from the unbroken chain in the frequency range of 30 Hz to 130 Hz. In the higher frequency range, it is difficult to distinguish between the broken and unbroken cases. From these results, using acoustic emissions systems for larger structural health monitoring needs further study.

There is significant variability in the acoustic emissions of the mooring chain, which is a result of a variety of factors. In each of these tests, the frequency spectra are compiled averages of 15 trials to limit the effect of outside background noise and the natural variability of the chain's acoustic emissions. Other sources of error in these test results may be a result of slight differences in the positioning of the microphone, which would likely impact the magnitude of the recorded AE. Additionally, noises within the laboratory may have slightly impacted testing results, however tests with noticeably loud interruptions, such as doors slamming or people walking by the testing space, were re-recorded.

The findings of these experiments led to the determination of common frequencies emitted from chain noise. However, due to the variability of the movements and interactions between links, the frequency spectrum for chain noise is not easily characterized. Therefore, it would be difficult to use this method of acoustic emissions monitoring to detect defects in mooring chain. Furthermore, these tests were performed in a lab environment where ambient noise was limited, and the movement of the chain was uniform across all tests. In application, acoustic systems would need to operate in water and filter ambient noises of waves, weather, boats, and animals, and determining this ambient spectrum would be much more complicated. The results of the 2-link unbroken and broken chain test in Figure 9 show that there is a possibility of frequency spectrum analysis indicating some type of failure in a chain if the AE a specific healthy system is known, however the 5-link unbroken and broken chain test in Figure 10 does not clearly lead to the same conclusion.

Turbine Generator Experiments

Figure 14 and Figure 15 display the frequency spectra for the two test conditions of the turbine generator experiments: uneven loading and tampered ball bearings. In both tests, there was a detectable difference in the sound of the fan when a fault case was induced. For the uneven loading case, increasing weight caused a lower vibrational humming noise. When salt was added to the bearings, a straining or "gritty" sound was audibly detected. These human-detected sounds are discernable from the following two figures.

Figure 14 displays the AE comparison of a fan with three different loading conditions: 0.05 g, 0.10 g, and 0.50 g. The spectrum for these tests appears as narrow spikes in frequency, as though they were tones. The healthy fan has large spikes at 120 Hz, 240 Hz, 330 Hz, and 360 Hz with

magnitudes of 5.5×10^{-5} V^2/Hz, 4.1×10^{-4} V^2/Hz, 4.8×10^{-5} V^2/Hz, and 8.0×10^{-6} V^2/Hz, respectively. Smaller spikes occur at 47 Hz, 234 Hz and 256 Hz, with magnitudes equal to 1.6×10^{-6} V^2/Hz, 2.6×10^{-6} V^2/Hz and 3.45×10^{-6} V^2/Hz, and these spikes do not occur for any of the loading cases. Furthermore, introducing loading caused spikes to occur at different frequencies. At 49 Hz, all three loading cases produced a spike that the unloaded fan did not. Additionally, the spike that occurred at 330 Hz for the unloaded fan shifted by 10 Hz to 340 Hz for all three loaded cases. The largest loading case, 0.50 g, produced spikes that the other loading cases did not at 97 Hz, 147 Hz, 169 Hz, 194 Hz, and 245 Hz. Lastly, the smallest loading case produced a spike at 217 Hz.

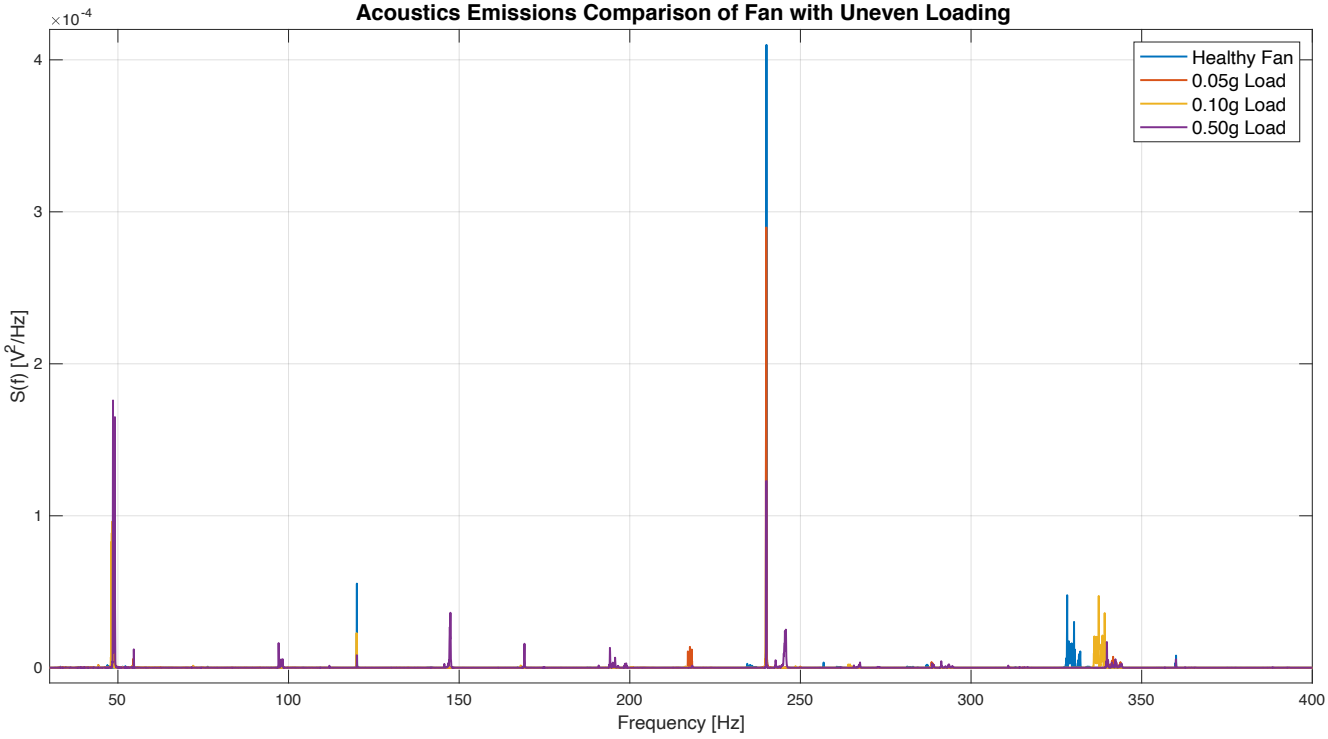

Figure 14: Frequency plot of fan AE with different loading conditions.

Also notable in Figure 14 is the change in magnitude of the spikes between loading conditions. At 120 Hz and 240 Hz, the magnitude of the spikes is greatest for the healthy fan. At 49 Hz, the spike that only occurs for the loading conditions, the magnitude increased as the load increased. A table of the notable frequency values and their magnitudes is shown in Table 6.

Table 6: Apparent Frequencies for Unevenly Loaded Fan.

Uneven Loading							
	Most Apparent Frequencies with Amplitudes						
Load (g)	47 Hz	49 Hz	97 Hz	120 Hz	147 Hz	169 Hz	194 Hz
0	$1.6\text{x}10^{-6}$ V^2/Hz			$5.5\text{x}10^{-5}$ V^2/Hz			
0.05		$1.7\text{x}10^{-6}$ V^2/Hz		$3.0\text{x}10^{-5}$ V^2/Hz			
0.1		$1.6\text{x}10^{-6}$ V^2/Hz		$2.5\text{x}10^{-5}$ V^2/Hz			
0.5		$1.6\text{x}10^{-6}$ V^2/Hz	$0.3\text{x}10^{-6}$ V^2/Hz	$1.3\text{x}10^{-5}$ V^2/Hz	$0.4\text{x}10^{-6}$ V^2/Hz	$0.3\text{x}10^{-6}$ V^2/Hz	$0.1\text{x}10^{-6}$ V^2/Hz
Load (g)	217 Hz	234 Hz	240 Hz	245 Hz	256 Hz	330 Hz	360 Hz
0		$2.6\text{x}10^{-6}$ V^2/Hz	$4.1\text{x}10^{-4}$ V^2/Hz		$3.45\text{x}10^{-6}$ V^2/Hz	$4.8\text{x}10^{-5}$ V^2/Hz	$0.5\text{x}10^{-6}$ V^2/Hz
0.05	$0.1\text{x}10^{-6}$ V^2/Hz		$2.9\text{x}10^{-6}$ V^2/Hz				$0.5\text{x}10^{-6}$ V^2/Hz
0.1			$1.6\text{x}10^{-6}$ V^2/Hz				$0.3\text{x}10^{-6}$ V^2/Hz
0.5			$1.6\text{x}10^{-6}$ V^2/Hz	$0.3\text{x}10^{-6}$ V^2/Hz			$0.1\text{x}10^{-6}$ V^2/Hz

Figure 15 displays the frequency spectrum of the comparison of a healthy fan to a fan with tampered ball bearings. Similar to the healthy fan results during the uneven loading test, spikes in frequency for the healthy fan occur at 47 Hz, 120 Hz, 240 Hz, 330 Hz, and 360 Hz. The spectrum for the tampered ball bearing case maintains spikes at all the same frequencies, except for a shift in frequency of 10 Hz from 330 Hz to 340 Hz. Other differences in the plots appear as changes in magnitude at 120 Hz and 240 Hz, where the power spectral density of the tampered ball bearing is increased, and at 360 Hz, where the power spectral density of the tampered ball bearing is decreased. These values and their magnitudes are organized in Table 7.

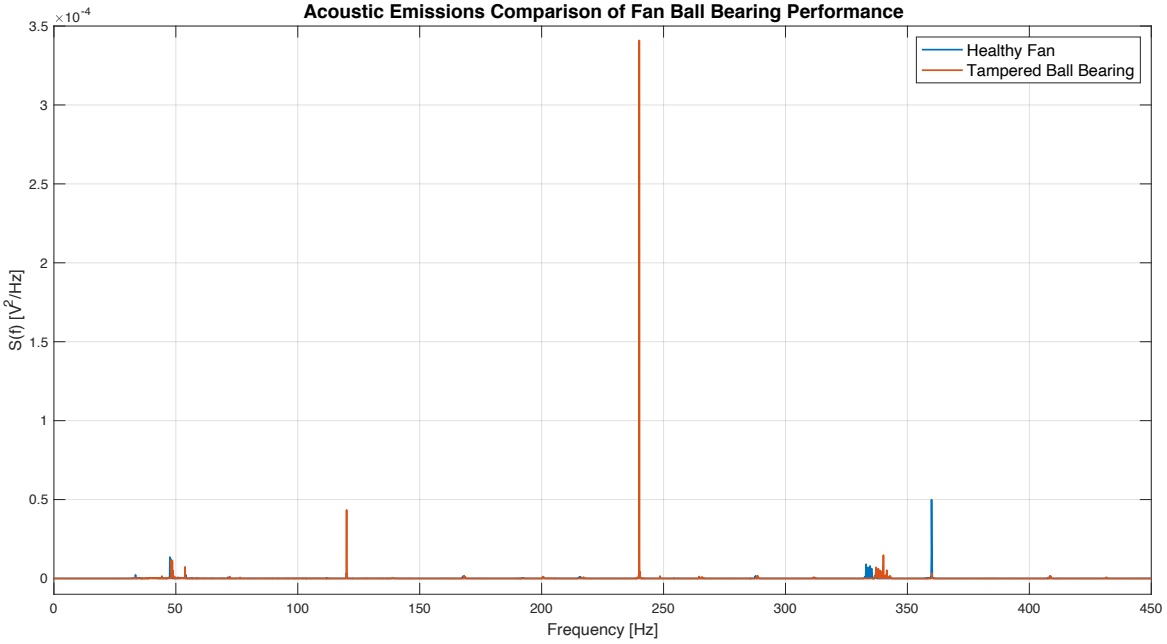

Figure 15: Frequency plot of fan AE before and after tampering ball bearings.

Table 6: Apparent Frequencies for Tampered Fan.

Tampered Ball Bearings						
	Most Apparent Frequencies with Amplitudes					
	47 Hz	120 Hz	240 Hz	330 Hz	340 Hz	360 Hz
Healthy	$1.6\text{x}10^{-6}$ V^2/Hz	$0.45\text{x}10^{-5}$ V^2/Hz	$3.4\text{x}10^{-4}$ V^2/Hz		$0.2\text{x}10^{-5}$ V^2/Hz	
Tampered	$1.6\text{x}10^{-6}$ V^2/Hz			$0.15\text{x}10^{-5}$ V^2/Hz		$0.5\text{x}10^{-5}$ V^2/Hz

The frequency spectra observed for the fan revealed greater potential for the use of AE for the structural health monitoring of the turbine generators in FWTs. Unlike a healthy chain, the healthy fan emitted a very predictable and repeatable spectrum of amplitudes and frequencies. The frequencies emitted by the fan were isolated to single frequency spikes at consistent amplitudes. It is likely that the frequency spikes are related to the fan's speed of rotation and number of blades, and several of the frequency spikes were harmonics of each other. For example, the healthy fan experienced a large spike at 120 Hz and smaller spikes at 240 Hz and 360 Hz, which are harmonics of the initial spike at 120 Hz.

When a defect was introduced into the fan, it manifested in the spectrogram as either an observable and isolated shift in frequency or change in amplitude. In Figure 14, it can be observed that introducing an uneven loading condition results in both a frequency shift and magnitude change. As the load increased, the magnitude of the original 120 Hz spike decreased, and unpredicted noise became apparent at different frequencies. The change in spectrums was a consequence of the fan's change in rotational patterns due to the uneven loading.

Uneven loading of one of the fan blades can be representative of an uneven load in other larger mechanical structures like a turbine generator. An unbalanced motor or generator could be the symptom of several failures like damaged bearings, defective belts, or worn machinery (Beleiu et al., 2022). These defects result in the unbalanced loading of the motor which will rotate and vibrate abnormally, emitting an unanticipated frequency. The findings in Figure 14 show that it could be possible to characterize the extent and severity of uneven loading because trends could be identified as the load increased. With increasing load, the spike that occurred at 330 Hz shifted to the right, revealing that the greater the shift in frequency, the greater the magnitude of the uneven load. In addition, the greater the load, the more frequency spikes occurred in new, unforeseen locations, revealing that the greater the load, the greater the array of frequency emissions.

Frequency and magnitude shifts can also be observed for the cases where the ball bearings of the fan were intentionally tampered with using salt. As shown in Figure 15, the tampered with fan introduced noise at 340 Hz and altered magnitudes of the emissions at 120 Hz and 240 Hz. These changes are also a reflection of the change in the fan's rotational behavior because of the defect. Since there was no way to modulate the severity of the damage to the ball bearings over multiple trials, it is difficult to draw any trends from the data, but it can be shown that the failure was detected both audibly to the human ear and in the spectrum of the AEs.

Conclusions

Mooring Chain Experiments

The goal of this project was to assess the feasibility of using acoustics for the structural health monitoring of floating wind turbines. Testing of different loading and chain length allowed for the conclusion that a chain in a lab setting will consistently produce spikes in certain frequencies. However, the magnitudes of these spikes vary, and other spikes occur randomly depending on the system. The two broken and unbroken test cases lead to inconclusive results that would require further testing to determine. The 2-link test indicates that there can be identifiable differences in acoustic emissions, however the 5-link test shows that this is not true for all cases. Based on these findings, there still may be potential for using AE systems for structural health monitoring, but it may not as reliable as needed for these large structures. However, it should be recognized that the test matrix for the feasibility study for acoustic monitoring of mooring chain was limited to small lengths of chains and small loads, and the findings could be different for different combinations of these parameters.

Turbine Generator Experiments

The findings of this project reveal greater potential for the use of AE monitoring for the structural health of rotating structures like larger generators and motors. Since the fan emitted such a consistent spectrum when subject to zero loading or failure modes, it was easier to detect when a defect occurs based on the changes to the spectrum. The ability to easily characterize the AEs of a healthy fan points to the ability to characterize the defects as well. If used to monitor the health of larger structural components like turbine generators and motors, AE monitoring could be able to identify the first case of abnormal behavior in a structure and be used to monitor its severity over time. Additional testing would be imperative to confirm the reliability of AE monitoring for use in FWTs.

Recommendations for Future Work

The goal of this project was to determine the feasibility of using acoustic emissions monitoring to detect changes in the structural health of offshore wind platforms. The experiments conducted addressed extreme conditions of breaking, movement, and ambient conditions. For mooring chain analysis, if using acoustic systems for monitoring were to be pursued, it is recommended that scaling the test chains and varying location (i.e. performing experiments underwater), closer simulation of chain movement in the natural environment, larger loads, and severity of defect is investigated in a laboratory. If findings from these tests indicate that there is a greater potential for AE monitoring than proven in these initial feasibility tests, it would be recommended that in situ tests be performed with an underwater acoustic monitoring system. The greatest challenge at that point would be detecting changes in AE over the ambient noise of the natural environment.

For the turbine generator experiments, next steps should include increasing the scale of the test generator and testing in situ to determine how ambient noise affects the detectability of changes to the generator performance. Because the changes in the turbine generator experiment were either magnitude changes or small shifts in frequency, it is unclear if these will be detectable in louder ocean environments.

Acknowledgements

This project could not have been done without the help of advisors Professor Thomas Weber and Professor Martin Wosnik at the University of New Hampshire. We additionally want to thank our industry partner, Jerica Nolte of Attentive Energy for her guidance and mentorship. This work was funded in part by New Hampshire Sea Grant's Workforce Development Project E/WFD-1, pursuant to National Oceanic and Atmospheric Administration Award No. NA18OAR4170090.

Appendix

Yeti Microphone Technical Specifications:

Microphone and Performance	
Power Required/ Consumption:	5V 150 mA
Sample Rate:	48 kHz
Bit Rate:	16-bit
Capsules:	3 Blue-proprietary 14 mm condenser capsules
Polar Patterns:	Cardioid, Bidirectional, Omnidirectional, Stereo
Frequency Response:	20 Hz – 20kHz
Max SPL:	120 dB (THD: 0.5% 1 kHz)
Dimensions (extended in stand):	4.72” (12 cm) x 4.92” (12.5 cm) x 11.61” (29.5 cm)
Weight (microphone):	12 lbs (.55 kg)
Weight (stand):	2.2 lbs (1 kg)

https://www.bluemic.com/en-us/products/yeti/#full-features

Fan Technical Specifications:

Product Identifications	
Manufacturer	AC Infinity Inc.
Product Name	AXIAL 1238
Product Model	HS1238A-X
UPC Code	854759004181
ASIN	B009OWRMZ6
Product Dimensions	
Total Dimensions	4.7 x 4.7 x 1.5 in (12.0 x 12.0 x 3.8 cm)
Hole to Hole Distance	4.13 x 4.13 in (10.5 x 10.5 cm)
Cord Length	48 in (4 feet)
Product Performance and Technical Specs	
Fan Model	HS1239A
Total Airflow	110 CFM
Total Noise	47 dBA
Speed	2600 RPM
Operating Voltage	100 to 120V AC
Power	18 W
Current	0.16 A
Static Pressure	9.1 mm-H20
Operating Humidity	35 to 85% RH
Operating Temperature	32 to 140 degrees F
Fan Bearings	Dual Ball
Mounting Positions	Horizontal or Vertical
L10 Life Expectancy	67,000 Hours

https://www.acinfinity.com/

MATLAB Code for microphone recording:

```
%Instructions for data collection:
%%%Run code section by section
%%%Code is for use with Yeti Stereo Microphone

%% Microphone initialize and record

info = audiodevinfo;

%Determine Input Device
    %info.input(1), info.input(2), ... info.input(n)
    %find 'Microphone (Yeti Stereo Microphone)

Fs = 22050;          %Hz, other standard values are 8000, 11025, 22050 Hz
bits = 24;           %other standard values are 8, 16, 24
channels = 1;        %2 channels available,
dev_id = 2;

arec = audiorecorder(Fs, bits, channels, dev_id);

samplelength = 15;    %seconds
```

```
arec.StartFcn = 'disp( ''Beginning of recording.'')';
arec.StopFcn = 'disp( ''End of recording.'')';

%% Ambient Noise
record(arec, samplelength)
pause(samplelength)

audioarray_amb = getaudiodata(arec);
t_amb = linspace(0, samplelength, length(audioarray_amb));

x = t_amb(t_amb<0.2);
audioarray_amb(1:length(x)) = [];
t_amb(1:length(x)) = [];

[pxx_amb, freq_amb] = periodogram(audioarray_amb, [], [], Fs);

%% Mooring Chain
record(arec, samplelength)
pause(samplelength)

audioarray_chain = getaudiodata(arec);
t_chain = linspace(0, samplelength, length(audioarray_chain));

x = t_chain(t_chain<0.2);
audioarray_chain(1:length(x)) = [];
t_chain(1:length(x)) = [];

[pxx_chain, freq_chain] = periodogram(audioarray_chain, [], [], Fs);

%% Plotting
subplot(3,1,1)
plot(t_chain, audioarray_chain,t_amb,audioarray_amb)
title('Microphone Recording in Time Domain')
xlabel('Time [s]')
ylabel('Voltage [V]')
legend('Chain', 'Ambient')
xlim([0.2 samplelength])

subplot( 3, 1, 2)
plot(freq_chain, pxx_chain,freq_amb, pxx_amb)
title('Microphone Recording in Frequency Domain');
xlabel('Frequency [Hz]');
ylabel('S(f) [V^2/Hz]');
xlim([0 Fs/2])
legend('Chain', 'Ambient')

subplot(3, 1, 3)
loglog(freq_chain, pxx_chain,freq_amb, pxx_amb)
title('Microphone Recording in Frequency Domain');
xlabel('Frequency [Hz]');
ylabel('S(f) V^2/Hz');
xlim([0 Fs/2])
legend('Chain', 'Ambient')
grid on
```

References

Abbelurg et al. (2014). *Project: Acoustic Monitoring of Floating Offshore Wind*.

ATB | NREL. (2022). NREL. https://atb.nrel.gov

Beleiu, H. G., Pavel, S. G., Birou, I. M. T., Miron, A., Darab, P. C., & Sallah, M. (2022). Effects of voltage unbalance and harmonics on drive systems with induction motor. *Journal of Taibah University for Science*, *16*(1), 381–391. https://doi.org/10.1080/16583655.2022.2064670

Electricity explained - U.S. Energy Information Administration (EIA). (2022, April 19). U.S. Energy Information Administration. https://www.eia.gov/energyexplained/electricity/

Ezzaidi, A., Elyaqouti, M., Bouhouch, L., & Ihlal, A. (2017). Evaluation of the Energy Performance of the Amougdoul Wind Farm, Morocco. *International Journal of Electrical and Computer Engineering (IJECE)*, *7*(2), 692. https://doi.org/10.11591/ijece.v7i2.pp692-705

Floating Offshore Wind Energy: A Policy Blueprint for Europe. (2016). https://windeurope.org/wp-content/uploads/files/policy/position-papers/Floating-offshore-wind-energy-a-policy-blueprint-for-Europe.pdf

Manz, B. (2020). *Wind Turbines: Tiny Sensors Play Big Role*. Mouser Electronics. Retrieved October 22, 2021, from https://www.mouser.com/applications/tiny-Sensors-Role-in-Wind-Turbines/

Martinez-Luengo, M., Kolios, A., & Wang, L. (2016). Structural health monitoring of offshore wind turbines: A review through the Statistical Pattern Recognition Paradigm. *Renewable and Sustainable Energy Reviews*, *64*, 91–105. https://doi.org/10.1016/j.rser.2016.05.085

Mba, D. (2006). Development of Acoustic Emission Technology for Condition Monitoring and Diagnosis of Rotating Machines: Bearings, Pumps, Gearboxes, Engines, and Rotating Structures. *The Shock and Vibration Digest*, *38*(1), 3–16. https://doi.org/10.1177/0583102405059054

NREL Learning. (2020, March 17). *Overview of Floating Offshore Wind* [Video]. YouTube. https://www.youtube.com/watch?v=58EYcYbRKqk&feature=youtu.be

Tang, J., Soua, S., Mares, C., & Gan, T. H. (2016). An experimental study of acoustic emission methodology for in service condition monitoring of wind turbine blades. *Renewable Energy*, *99*, 170–179. https://doi.org/10.1016/j.renene.2016.06.048

Tonelli, D., Luchetta, M., Rossi, F., Migliorino, P., & Zonta, D. (2020). Structural Health Monitoring Based on Acoustic Emissions: Validation on a Prestressed Concrete Bridge Tested to Failure. *Sensors*, *20*(24), 7272. https://doi.org/10.3390/s20247272

Bailey, H., Brookes, K., Thompson, P., (2014). Assessing environmental impacts of offshore wind farms: lessons learned and recommendations for the future. *Aquatic Biosystems.* 9. https://www.researchgate.net/publication/266086383